NTNU
Norwegian University of
Science and Technology

Simulation of Two-Phase Flow in Porous Media using a Network Model.

Eivind Eskerud Harris

Master of Science in Physics and Mathematics
Submission date: December 2016
Supervisor: Alex Hansen, IFY

Norwegian University of Science and Technology
Department of Physics

Abstract

A network simulator has been used to study two-phase flow in porous media. The medium has been modeled as a bundle of tubes and the capillary forces inside these tubes have been investigated. This has been done by applying well known theory of immiscible flow to tubes of different shapes. How the wettabillity of the media affect the meniscus curvatures have been studied and how this relates to the cross-section geometry and width of a single tube. The tube radius was modeled by a function being narrow in the middle of the tube and wider towards the end. How the menisci was affected by this curvature due to varying radius have been investigated. Different degrees of complexity have been used to see if simple approximations are able to capture the relevant physics or if a higher order of complexity is needed.

It was found that the cross-sectional shape does not have a big impact on the flow, however thin film flow was neglected. When looking at how the radius affected the results it was found that approximations used in previous work was sufficient for small wetting angles, however at large wetting angles this expression became inaccurate. Finally different radius functions were tested to see if the shape of the radius had any impact. Some differences were observed but it is hard to conclude which case was the most physically correct due to lack of experimental data.

Sammendrag

En nettverkssimulator har blitt brukt til å studere tofasestrømning i porøse medier. Mediet har blitt modellert som et sett med sammenhengende rør og kapillærkreftene i disse rørene har blitt undersøkt. Dette har blitt gjort ved å anvende kjent teori om tofasestrømning på rør med ulike geometrier. Hvordan mediets fuktning påvirker meniskens krumning har blitt undersøkt og hvordan dette henger sammen med geometri på tversnitt og bredde på rør. Radiusen på røret ble modellert som en funksjon som var smal på midten og bred på endene. Hvordan meniskene ble påvirket av det krumme røret ble undersøkt. Ulik grad av kompleksitet ble brukt for å se om enkle tilnærminger er gode nok til å beskrive de relevante fysiske prosessene, eller om mer avanserte tilnærminger er nødvendig.

Resultatene viste at formen på tverrsnittet hadde lite innvirkning på strømningen, men det er viktig å nevne at filmstrøm ble neglisjert. Ved å se på hvordan radiusen påvirket resultatet viste det seg at for små fuktningsvinkler var de tilnærmninger som har blitt brukt i tidligere arbeid gode men når fuktningsvinkelen nærmet seg 90° ble de mindre presise. Til slutt ble ulike radiusfunksjoner testet for å se om dette hadde innvirkning. Det var enkelte forskjeller, men manglende eksperimentell data gjør det vanskelig å si hvilke som er mest korrekt.

Preface

This thesis has been submitted as a final part of my masters degree in Applied Physics and Mathematics at NTNU. I would like to thank Morten Vassvik for valuable help during this period. I would also like to thank Alex Hansen, Signe Kjelstrup and the rest of the PoreLab at NTNU for valuable feedback and discussions.

Table of Contents

List of Figures

Chapter 1

Introduction

Flow phenomena in porous media has been an important research topic for decades and it arises in many fields of science such as agricultural, biomedical, construction and petroleum engineering. Ground water is a precious resource, but it can easily be contaminated. The New York Times (2016) wrote that China's biggest pollution problem is not the city smog, but polluted ground water. As much as 80 % of the ground water used for farming and household in rural areas is contaminated and unfit for drinking. A better understanding of how chemicals are transported in groundwater reservoirs can help preventing this pollution from happening. In the petroleum industry knowledge about how oil and water flows in the ground is important. When draining oil reservoirs, a lot of oil gets trapped within porous rocks, and retrieving this oil in an efficient way is not an easy task.

A porous medium such as sand stone consists of microscopic spherical rocks packed close together. In between the rocks there are small pores and narrow paths. Two phase flow within such a medium is a complicated process. This is mainly due to the complex structure of the pores, and the interfaces between the immiscible fluids trapped inside. Various experimental, computational and theoretical methods have been developed to investigate the behaviour of such flow. Theoretical models can predict flow patterns in certain cases, but are limited in many ways. Computational methods have been quite successful in describing the two phase flow, but it is a challenge to find feasible techniques who are computationally inexpensive and physically correct. Experiments are very valuable. They can be analyzed to get a deeper understanding of the physics behind the flow process, and verify computational and theoretical results. Accurate measurements are a challenge and performing the experiments can be time consuming, thus one can say that experiments and simulations complement each other.

Several computational models for two-phase flow has been developed. According to the review article by Joekar-Niasar and Hassanizadeh (2012) they can be split into two groups, continuum-scale models and pore scale models. The continuum models are not able to explain the consequence of microscopic properties on a macroscopic scale. Because of this they fail to explain phenomena such as viscous fingering and similar invasion processes. In order to capture the effect of microscopic properties such as pore geometry, capillary

forces and viscosity, pore scale models must be used. There are several subgroups of these models, and two important ones are Lattice Boltzmann models and network models.

Lattice Boltzmann models (e.g Knutson et al. (2001), Martys and Hagedorn (2002)) solves Navier Stokes equation for a given pore geometry and is quite accurate. However, this is computationally expensive and an infeasible approach if doing large scale simulations. Network models however are computationally less expensive, but relay on a simplified model of the porous medium and thus some geometrical information is lost. A common way to model a porous medium in a network model is by considering pore bodies and connecting throats (e.g Dias and Payatakes (1986)). Another way is to let a tube with varying width model both the pore and the throat between them. This has been done by Aker et al. (1998), Knudsen and Hansen (2002) and Valavanides et al. (1998).

The work in this thesis is based on the model developed by Aker et al. (1998). Here hourglass-shaped tubes were used to model the pores. An approximation for the capillary pressure difference was found based on this shape. Significant improvements have been made to this model since it was first published, however how the geometry of each tube affect the simulation results have not been investigated in detail. The purpose of this work is to study how the tube geometry affect the local capillary pressure, which again may affect the macroscopic properties of the system. It will also look into if some of the approximations that have been made in the past are sufficient, or if a higher order approximation is needed to capture the relevant physics. To do so several cases with different geometries will be studied and compared. A reimplementation of the basic simulation procedure has been done in c++. Some modifications has been made to include the new geometric features.

This thesis will be organized the following way: Chapter 2 will present the basic theory that is applied in the network model, while chapter 3 will explain the details behind the implementation of the system and how the simulations are carried out. Chapter 4 will present the results for several realizations where different approximations and models have been used and discuss them. Chapter 5 will draw the final conclusions.

Chapter 2

Theory

This chapter will present the basic theory needed to describe two phase flow in porous media. First a description on how a porous medium can be modeled as a bundle of capillary tubes will be given. Then the focus will be the capillary forces and flow rates inside these tubes. The effect of tube geometry will be studied in detail. The final part will briefly present the theory used to describe the macroscopic behavior and displacement mechanics that is observed in these systems.

2.1 Modeling a Porous Medium

The behavior of immiscible wetting and non-wetting fluids in a porous medium depends on the geometry and topology of the medium. In general, this geometry can be very complex, and simplifications must be made to create a model that can be used in network simulations. Øren and Bakke (2002) has developed methods of reconstructing a porous sandstone and use this reconstruction to make a realistic network model. In this work however a simple 2D network topology will be used, namely a hexagonal lattice. To illustrate why this is chosen look at figure 2.1 a), which illustrates a typical geometry of a porous medium. The basic idea behind the modelling is to treat each pore as an intersection between tubes, where each tube connects one pore to another. This can be seen in figure 2.1 b). Here the tubes have varying length and radius. To simplify further it is assumed that the length of each tube is the same. This results in a geometry like figure 2.1 c), which is a hexagonal lattice. This is a simple model, but the goal is not to study the effect of network structure, and thus this simple model is chosen to avoid unnecessary complexity. Note that in this case both the pore body and the pore throat is modeled by the same tube.

The shape of the tube's cross section does have significance, and several cases have been studied in the literature. The simplest one is the circular cross section used by Fatt et al. (1956). Mason and Morrow (1991) used a triangular shape, while Fenwick et al. (1998) used a square. A star shaped tube was used by Man and Jing (2000). By looking at figure 2.2 which illustrates the space between three spherical objects, it is seen that triangular shaped tubes are quite accurate if choosing from basic geometrical shapes. In the rest of

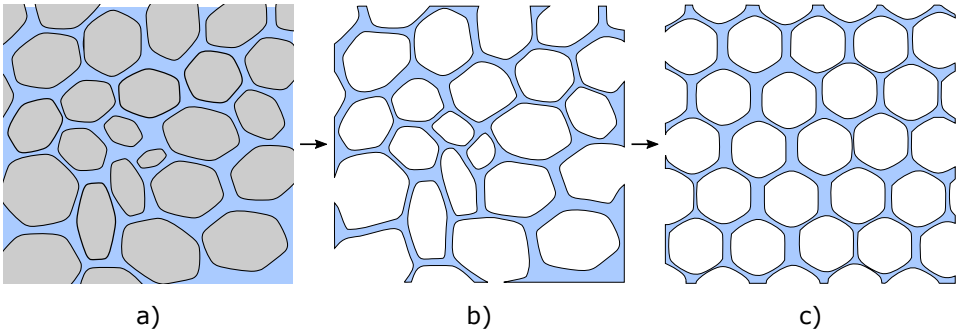

Figure 2.1: How a porous media can be modeled as connecting tubes. a) illustrates the real porous media, b) shows the equivalent grid of tubes with varying length and c) shows the case where all tubes have the same length.

this chapter both cylindrical and triangular shapes will be studied.

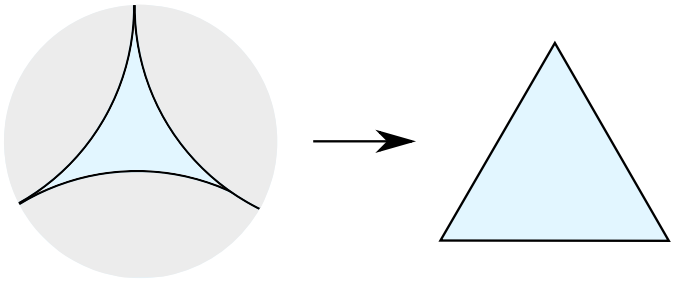

Figure 2.2: Illustration of how a the cross section of a porous tube can be modeled as a triangle

2.2 Wetting and Capillary Forces

The interface between the immiscible fluids inside the porous medium is of great importance because capillary forces will arise due to different wettabillity of the two fluids. Wettability describes ”the preference of a solid to be in contact with one fluid rather than another” (Schlumberger (2007)). This means that when having a wetting and non-wetting fluid in a container, the wetting one will be more attracted to the walls than the non-wetting one. This will result in a curved interface between the fluids called a meniscus. An important parameter when characterizing the properties of these interfaces is the wetting angle. The wetting angle is the angle at which the liquid and solid interfaces intersect. A wetting liquid will have a high wetting angle while a non-wetting liquid will have small wetting angles. This is shown in figure 2.3.

At the intersection between immiscible fluids with different wetteabillity, a pressure difference will occur. This is known as the capillary pressure difference and is described by

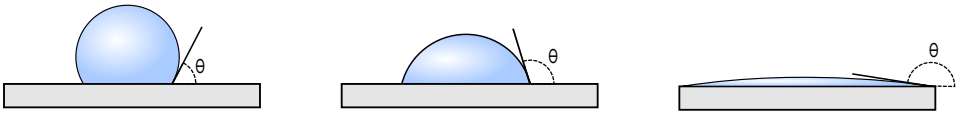

Figure 2.3: The behaviour of a liquid with different wetting angles

the Yong-Laplace law (Sahimi (2011)),

$$p_c = \pm\frac{2\gamma}{R} = \pm\frac{2\gamma}{r}\cos(\theta). \tag{2.1}$$

Here γ is the surface tension between the fluids and the wall, R is the radius of curvature for the meniscus, and θ is the wetting angle. r is the radius of the circular surface were the solid and liquid intersect and the sign is given by the way the meniscus is turning.

2.2.1 Capillary forces in straight tubes

To understand the effect of capillary forces in a porous medium at a macroscopic scale we must start looking at the meniscus behaviour in each tube in the network. As stated by (2.1) the capillary pressure is directly proportional to the curvature of the meniscus. The meniscus curvature will depend on the geometry of the tube. This includes both cross-sectional shape and tube width. For cylindrical tubes with constant cross sections the capillary pressure is simply given by the Young-Laplace law (2.1), where r now is the radius of the tube. Tubes with triangular cross sections will also be studied in this work. It is not trivial to find the capillary pressures in such tubes. This has been done by Mason and Morrow (1991), and developed further by Øren et al. (1998). What is presented in this section is taken from these articles. The geometry factor G is a useful quantity when describing triangular tubes, and is defined as

$$G = \frac{A}{P^2}, \tag{2.2}$$

where A is the area of the cross section and P is the perimeter. The geometry factor can also be described by the half angles of the triangle corners β_i,

$$G = \frac{1}{4}\left(\sum_{i=1}^{3}\cot\beta_i\right)^{-1} \tag{2.3}$$

When fluids with different wettability are inside the same triangular tube the wetting fluid will be drawn towards the corners of the triangle while the non-wetting fluid will be occupying the center of the tube. This is illustrated in figure 2.4. The surface that separates the fluids along the axis of flow is called the Main Terminal Meniscus (MTM) while surface which separates the fluid in the corners is called the Arc Meniscus (AM). These are shown in figure 2.4. For geometries like this the Ms-P approach, proposed by Lenormand et al. (1983), is a commonly used technique to find the curvatures of the meniscus and thus the

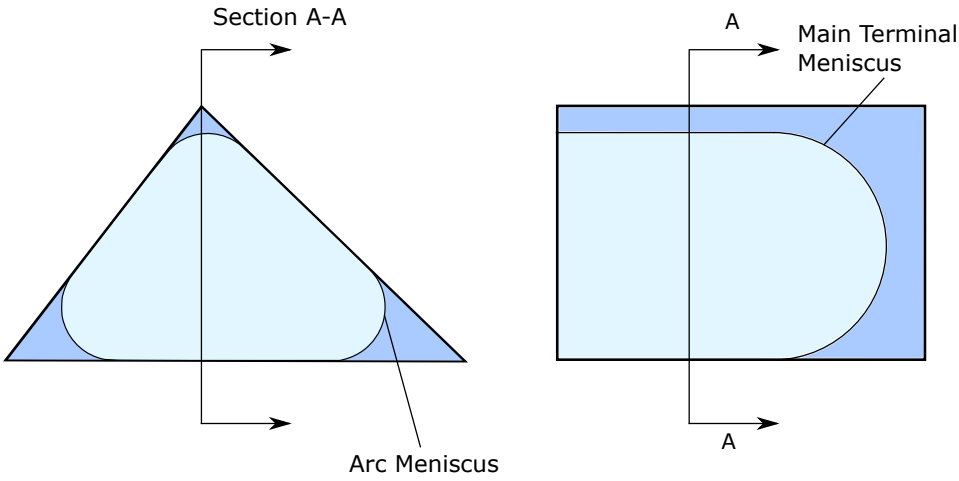

Figure 2.4: Illustration of the meniscus geometry in triangular tubes

capillary pressure. The basic idea is to equate the curvatures of the AM and MTM, solve this equation to find the radius of curvature. For a general triangular tube with zero wetting angle the Ms-P approach yields.

$$p_c = \frac{\gamma}{r_{\text{inc}}} \left(1 + 2\sqrt{\pi G}\right) \tag{2.4}$$

This can be extended to include the wetting angle, resulting in a pressure

$$p_c = \frac{\gamma}{r_{\text{inc}}} \left(1 + 2\sqrt{\pi G}\right) \cos\theta F(\theta, G) \tag{2.5}$$

where

$$F(\theta, G) = \frac{1\sqrt{1 - 4GE/\cos^2\theta}}{1 + 2\sqrt{\pi G}} \tag{2.6}$$

$$E = \sum_{i=1}^{3} \cos\theta \frac{\cos\left(\theta + \beta_i\right)}{\sin\beta_i} - \left(\frac{\pi}{2} - \theta - \beta_i\right) \tag{2.7}$$

Here r_{inc} is the radius of the inscribed circle in the triangular cross section. This expression is only valid for wetting angles

$$\theta < \frac{\pi}{2} - \beta \tag{2.8}$$

It is worth noting that $F(\theta = 0, G) = 1$. For a fixed value of G the value of F changes little for varying θ, thus the approximation

$$p_c = \frac{\gamma}{r_{\text{inc}}} \left(1 + 2\sqrt{\pi G}\right) \cos\theta \tag{2.9}$$

can be used. The real and approximated values are plotted in figure 2.5. The physical interpretation of this approximation is that the curvature of the AM is kept constant while

only the MTM is varying. When using this approximation, the shape of the p_c curve is the same for circular and triangular cross sections, the only difference is a scaling factor $1 + 2\sqrt{\pi G}$,

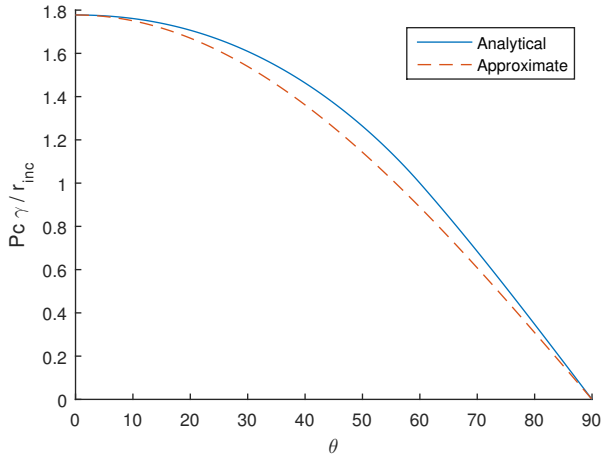

Figure 2.5: How the capillary pressure depends on θ, for triangular tubes. The blue line is the full analytical expression while the red line shows the approximation where $F = 1$

2.2.2 Capillary pressures in tubes of varying radius

So far tubes with constant cross sections have been considered, but in order to make the model more realistic tubes of varying widths should be used. In particular tubes which are narrow at the middle and getting wider towards the ends. This is illustrated in figure 2.6. Note that throughout this thesis the radius is only varying with respect to the capillary pressures. When calculating flow rates the volume of a straight tube with constant cross section will used. This kind of geometry has implications on the capillary pressure, because the wetting angle is now the angle between the slope of the tube and the meniscus. One immediate observation is that a wetting angle of 90° no longer corresponds to zero capillary pressure. In the preceding discussion the radius will be described as a function of the coordinate x. Inside the tube we will have $0 \leq x \leq L$. The radius function $r(x)$ will always be symmetrical about $x = L/2$. For cylindrical tubes with this type of radius function Oh et al. (1979) has shown that the radius of curvature of the meniscus is given by.

$$R(x) = \frac{r(x)}{\cos(\theta - \alpha(x))}, \tag{2.10}$$

where $\tan(\alpha) = r'(x)$, thus α is the angle between the slope of the tube and the horizontal axis. The capillary pressure now becomes,

$$p_c = \frac{\gamma}{r(x)} \cos(\theta - \alpha(x)). \tag{2.11}$$

This is illustrated in figure 2.6. For triangular tubes this gets more complicated because

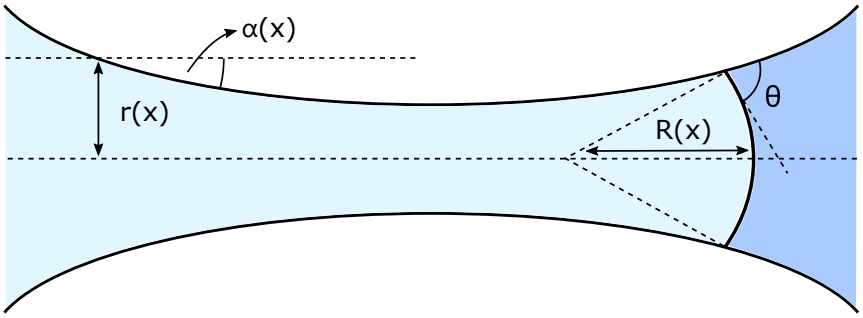

Figure 2.6: Relevant parameters for a meniscus inside a tube of varying radius.

the curvature of the AM as well as MTM will be affected by the change of width. However if the AMs curvature is assumed to be constant equation (2.9) can be extended in the same manner as for cylindrical tubes,

$$p_c = \frac{\gamma}{r_{\text{inc}}(x)} \left(1 + 2\sqrt{\pi G}\right) \cos(\theta - \alpha(x)). \tag{2.12}$$

Here it is assumed that the corner angles of the tube are kept constant while the width is changing.

So far $r(x)$ has been considered as an arbitrary function. It should be chosen so that the tube shape resemblances the path between two pores in a porous medium. Aker et al. (1998) used an approximation for the capillary pressure,

$$p_c = \frac{2\gamma \cos\theta}{r} \left(1 - \cos\left(\frac{2\pi x}{L}\right)\right). \tag{2.13}$$

If the angle of the slope α is not taken into account this would correspond to the radius

$$r(x) = \frac{r_0}{1 - \cos\left(\frac{2\pi x}{L}\right)}. \tag{2.14}$$

To study the effect of including the slope equation 2.14 will be used in 2.12. This radius diverges towards the ends of the tube which is not physical. A more realistic radius function that will be considered is the radius of a tube which lies between to circles. This shape can be modeled as

$$r(x) = \frac{1}{2}(r_0 + L) - \sqrt{xL - x^2}. \tag{2.15}$$

The constant term is chosen such that the narrowest part in the tube will have the same radius as in (2.14).

When using the previously mentioned radius functions to calculate p_c there are some

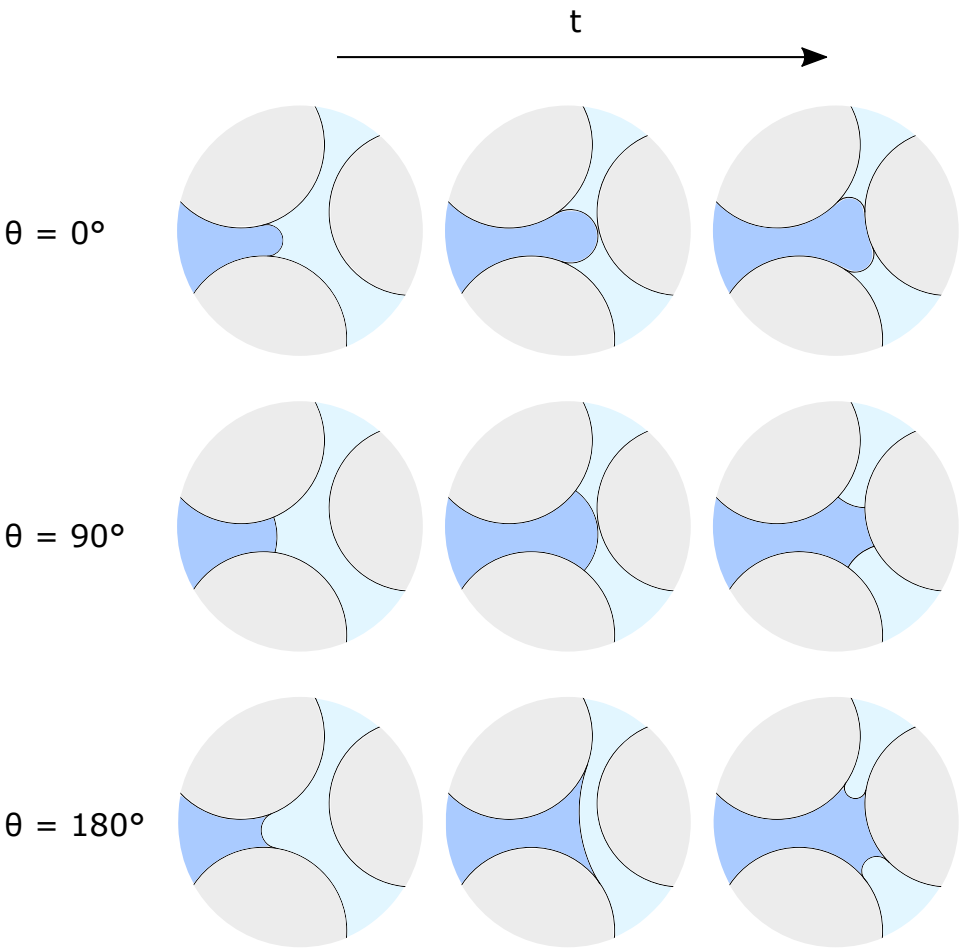

Figure 2.7: A meniscus of different wetting angles propagating through a node.

physical phenomena which are not being captured. Figure 2.7 shows the time evolution for a meniscus front entering a node, with three different wetting angles. Here the porous medium is modeled by circles and (2.15) will be used as radius function. In a porous medium the radius of curvature of a meniscus is allowed to vary as the meniscus travels through the tube. When the meniscus is about to exit, it will hit the wall on the other side of the node, preventing it from growing any further. This means that in many cases the capillary pressure will not drop to zero inside the node. This maximum radius of curvature will depend on the wetting angle of the meniscus. This is illustrated in figure 2.7 where it is seen that for $\theta = 0^\circ$ the curvature is heavily bounded, while in the opposite case, $\theta = 180^\circ$ the curvature is allowed to drop to zero. If the tubes are wide, it is possible that the meniscus can move beyond the point of zero curvature, and thus the p_c will switch sign, but this effect is not taken into account in the model that has been developed.

The task becomes now to find when the meniscus will reach its maximum radius of curvature within the node. In appendix A1 it is show that the position of the front of the meniscus is given by,

$$x_m = x + \frac{1 - \sin(\theta - \alpha(x))}{\cos(\theta - \alpha(x))} r(x), \tag{2.16}$$

where x is the position where the meniscus intersects with the wall. Note that the wetting angle is measured with respect to the most wetting fluid. Now that the meniscus position is established, we must find when it will hit the wall. To find an approximation to this, it is assumed that the radius of all the tubes connected to the relevant node is the same, and is set to an average $\bar{r}$. It is show in appendix A2 that the position along the x-axis where the menisci will hit the wall to the right is given by

$$x_r = \sqrt{3}\left(\frac{L}{2} + \bar{r}\right), \tag{2.17}$$

while the left position is given by

$$x_l = L - \sqrt{3}\left(\frac{L}{2} + \bar{r}\right). \tag{2.18}$$

These parameters are illustrated in figure 2.8

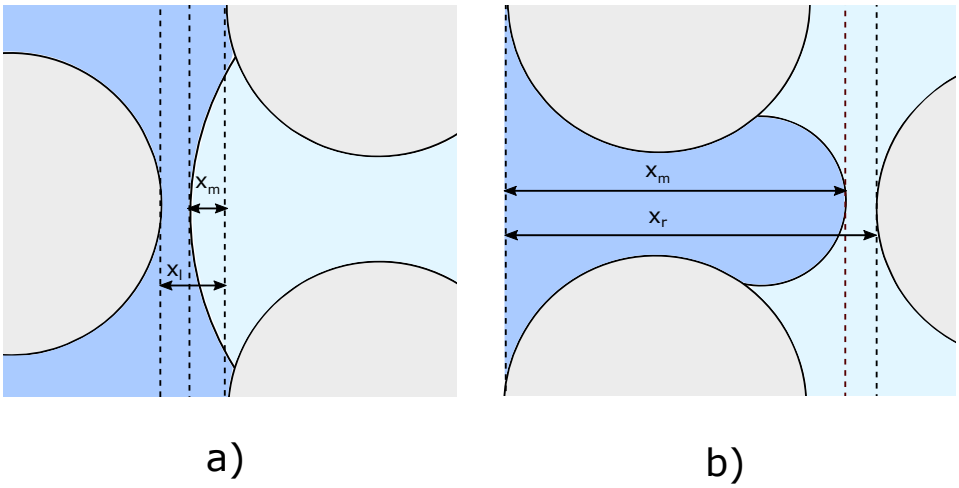

Figure 2.8: The relevant parameters to calculate the minimum meniscus curvature. To the left a meniscus entering a tube is illustrated, while to the right the meniscus is exiting the tube.

To find the maximum radius of curvature at both left and right side of the tube equation (2.16) can be set equal to (2.18) and (2.17) and solved with respect to x. This is not possible to do analytically, but can be solved numerically. Denoting these values $x_{\max}$ and

$x_{\min}$, the capillary pressure can finally be written as

$$p_c(x) = \begin{cases} f(x_{\min}) & 0 \leq x \leq x_{\min} \\ f(x) & x_{\min} < x < x_{\max} \\ f(x_{\max}) & x_{\max} \leq x \leq L \end{cases} \tag{2.19}$$

where $f(x)$ refers to equation (2.12) using the radius function (2.15) Here it is assumed that once the p_c has reached its threshold, it remains constant throughout of the remaining tube.

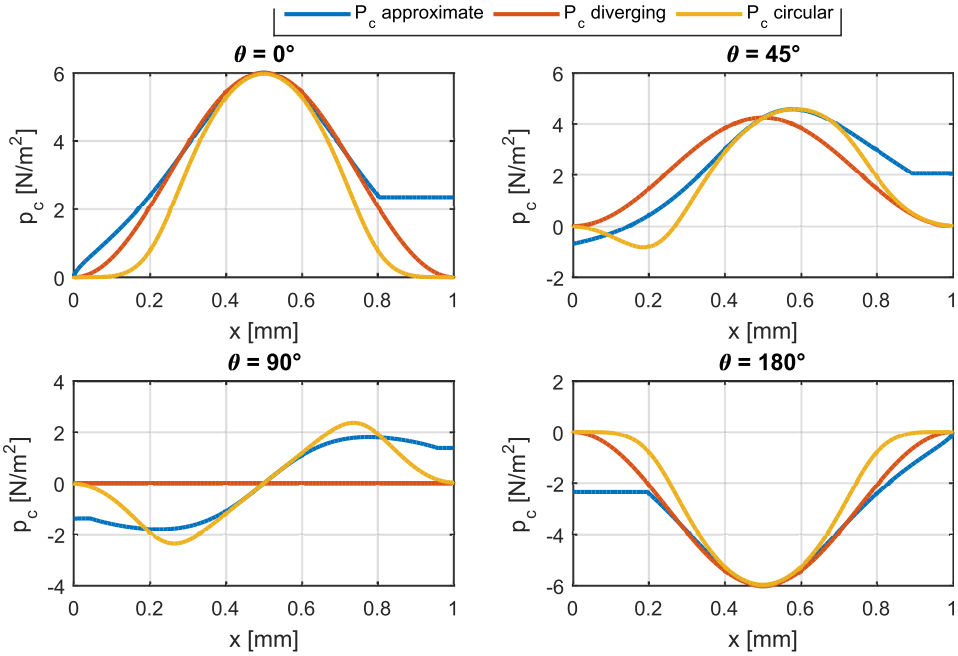

Figure 2.9: Capillary pressures as function of meniscus positions, for different wetting angles and menisci approximations

To compare the three different expressions for p_c they have all been plotted in 2.9 for wetting angles $0°, 45°, 90°$and $180°$. In the case of circular tube the capillary pressure bound has been applied. It is seen that for small wetting angles, (2.13) is a quite good approximation to the more realistic capillary pressure. However, as the wetting angle changes, the approximation becomes less accurate since the slope of the tube is not taken into account. The curves generated for the bounded capillary pressure stands out because it has a cutoff value. It is seen that for small wetting angles the p_c is only cut off at the end of the tube, but for wetting angles close to $90°$, the curve is completely symmetric about $x = 0.5$, and cut off at both ends. It is also seen that the maximum capillary pressure no longer lies in the center of the tube. The shape is similar to the one generated using the diverging radius function, but for this case the p_c still drops to zero at the endpoints. For

$\theta = 180°$ all curves are mirrored about the x and y axis compared to the curves with zero wetting angle. This makes sense, because a wetting angle $180°$, can be interpreted as if the wetting and non-wetting fluid has switched place.

2.3 Flow through tubes

In this thesis a steady state Newtonian, incompressible and constant viscosity fluid will be assumed. According to Patzek and Silin (2001) the flow will then be governed by the elliptic Poisson equation

$$\nabla^2 \boldsymbol{v} = \frac{1}{\mu}(\nabla p - \rho \boldsymbol{f}) \tag{2.20}$$

Here $\boldsymbol{v}$ is the fluid velocity μ is the viscosity and ρ is the density. $\boldsymbol{f}$ is the body force per unit mass. Solving this equation with respect to the flow rate Q for a cylindrical tube results in (White (2011)),

$$Q = -\frac{kA}{\mu L}\Delta p. \tag{2.21}$$

Here μ the viscosity and k is the permeability which is a geometric quantity. The value of k is depending on the geometrical shape of the cross section of the tube. For cylindrical tubes we have

$$k = \frac{r^2}{8}, \tag{2.22}$$

and $A = \pi r^2$. For triangular tubes Patzek and Silin (2001) has shown that the mobility is approximately

$$k = \frac{3}{5}\frac{GA}{\mu}. \tag{2.23}$$

These expressions are only valid for single phase flow, but they can be extended to two

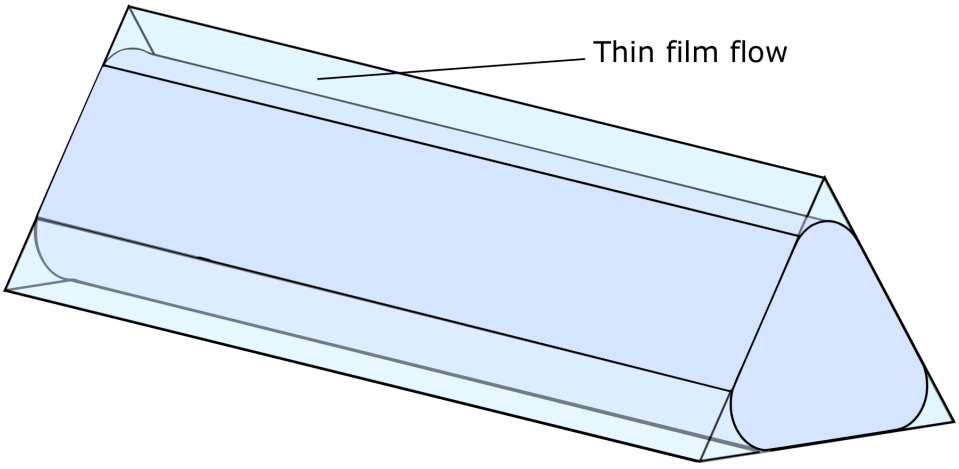

Figure 2.10: Thin film flow that occurs in the corners of a triangular tube

phases (Washburn (1921)). Treating the fluids as separate and applying equation (2.21) on both of them results in the flowing expression

$$Q = -\frac{kA}{\mu_{\text{eff}} L} \left(\Delta p - p_c \right), \tag{2.24}$$

where μ_{eff} is the weighted average of the two viscosities.

In the general case it is possible that both wetting and non-wetting fluids are flowing through the same cross section simultaneously. This would be the case for triangular pipes where it is possible that the wetting fluid will flow in the corners and the non-wetting in the center. The majority of the flow will be due to the non-wetting fluid and the wetting flow in this case will be referred to as thin film flow. In the proceeding analysis this flow will be neglected, thus is it assumed that only one kind of fluid flows through a cross section at a given time.

2.4 Macroscopic properties

So far flow in a single tube has been studied, but the focus of this thesis is what happens when these tubes are connected to each other in a grid. To characterize the flow phenomena that occur in a system like this it is useful to define several quantities. The saturation S refers to the fraction of the total pore volume which is occupied by either the wetting or non-wetting phase, denoted respectively S_{w} and S_{nw}.

The total volume flow through the medium per time unit is denoted Q. Due to conservation of flow it is arbitrary where this is measured, as long as it measured along a curve representing a close loop. In two phase flow this flow can be split into two parts, namely the flow of the wetting phase Q_{w} and non-wetting phase Q_{nw}. The fractional flow can be defined as

$$F_{\text{nw}} = \frac{Q_{\text{nw}}}{Q_{\text{w}} + Q_{\text{nw}}} \tag{2.25}$$

which is the fraction the total flow which is due to the non-wetting phase.

Darcy's law (Sahimi (2011)) relates the flow through a porous medium to its permeability and the pressure gradient in the medium,

$$Q = -\frac{\kappa \Sigma}{\mu} \Delta P. \tag{2.26}$$

In this case gravity has been neglected. ΔP is the total pressure gradient. Note that the permeability κ is the permeability of the whole medium and not just a single tube as in (2.21). In the case of constant ΔP and μ the permeability is proportional to the flow.

Understanding the interaction between the viscous and capillary forces is crucial when explaining the different flow patterns occurring in porous media. The capillary number describes the relation between these forces. In a flow with small capillary number the

capillary forces are dominating while large capillary numbers mean that the viscous forces are dominating. For a single tube the capillary number is defined as

$$C_a = \frac{\mu V}{\gamma}, \tag{2.27}$$

where μ is the fluid viscosity, V is the fluid velocity and γ is the interfacial tension. This equation only describes the flow in one single tube and can thus not be directly extended to two phase flow in a porous medium. Several definitions have been used. In the review article by Joekar-Niasar and Hassanizadeh (2012) the following definition were used

$$\mathrm{Ca} = \frac{\mu_i q_i}{\gamma}. \tag{2.28}$$

Here μ_i refers to the viscosity of the invading phase, q_i is the Darcy velocity of the invading phase and σ_{nw} is the interfacial tension between the fluids. The Darcy velocity refers to the total flow divided by the area of the pores in the cross-section where the flow was measured. This definition is a popular choice when studying invasion processes, but in this work the boundary conditions allow the fluid that exits the top of the network to reenter at the bottom, thus this becomes a mixing process, and not an invasion. Aker et al. (1998) used the following definition,

$$\mathrm{Ca} = \frac{Q\mu}{\Sigma\gamma}. \tag{2.29}$$

Here Q denotes the total flow rate and Σ is the total area of the cross section where the fluid enters and μ is the maximum viscosity. γ is the same as before, the interfacial surface tension. This is a more reasonable definition for our case because it uses the total flow rate and not just the invading one. None of the definitions above has explicit dependence on the wetting angle θ. Lenormand et al. (1988) used the definition

$$\mathrm{Ca} = \frac{\mu_i Q_i}{\Sigma\gamma_{nw}\cos\theta.} \tag{2.30}$$

Note that this expression is diverging as the wetting angle approaches 90 °. All these definitions give slightly different values of the Ca. The exact value of the capillary number is not that important. What we are interested in is its order of magnitude. For the rest of this work 2.29 will be used where Σ will be the pore volume where the flow is measured.

The viscosity ratio is defined as

$$M = \frac{\mu_1}{\mu_2} \tag{2.31}$$

where μ_1 and μ_2 is the viscosity of the wetting and non-wetting fluid respectively.

2.5 Displacement mechanics

Drainage is the process where the non-wetting fluid displaces the wetting fluid in a porous medium. This has been studied in detail in the last decades. The fluid flow can be divided into three different regimes, viscous fingering, stable displacement and capillary fingering.

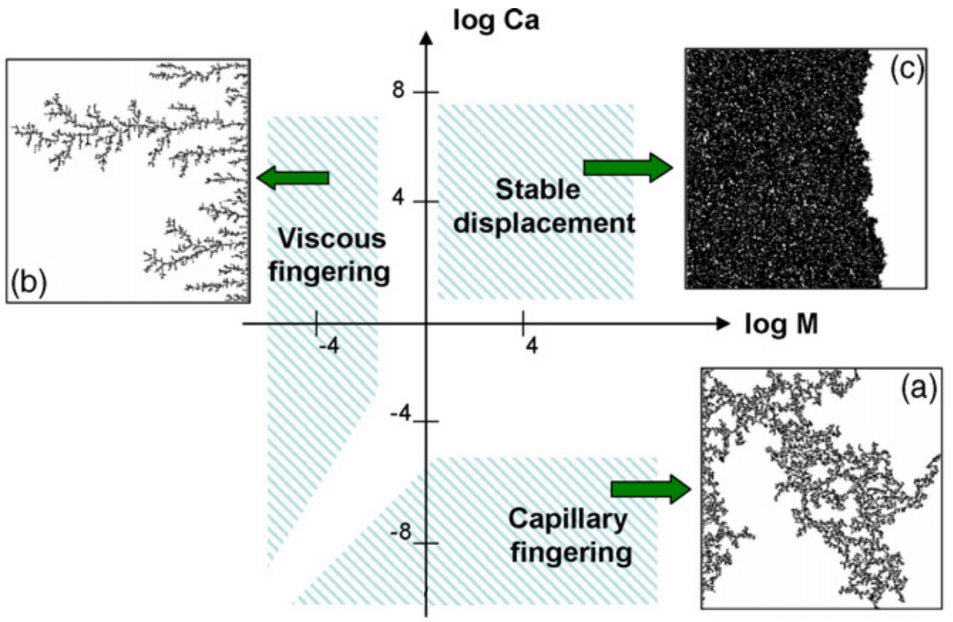

Figure 2.11: Flow patterns for different capillary numbers and viscosity ratios. Courtesy of Sinha and Wang (2007)

Lenormand et al. (1988) introduced a phase diagram describing these regimes in terms of the capillary number and viscosity ratio. This diagram is shown in figure 2.11. A lot of effort has been put into creating statistical models describing different flow regimes in porous media. This section will present a brief overview of the different methods.

Viscous fingering occurs when the viscosity ratio is small. The flow pattern can be seen in 2.11 b) and looks almost like a branching tree. Paterson (1984) discovered that there are great resemblances between diffusion-limited aggregation and viscous fingering. DLA is the process where a set of particles are allowed to move randomly one at the time away from an initial particle at a specific location. Once one of the moving particles hits a fixed particle it sticks to it, and thus this structure grows. The formation that is created is similarly to viscous fingering.

Stable displacement is the case when a fluid of high viscosity is displacing a fluid of low viscosity, opposite of viscous fingering this is illustrated in figure 2.11 c). The injection rate is assumed to be high, and thus the capillary forces are negligible. The characteristics of this flow is a stable front of invading fluid, with some roughness on the edge due to variations in the pore radius. This process is similar to anti-DLA. This is the process where a compact set of particles, which in this case represent the defending fluid, and particles undergoing random walk close by. Once the random walker collides with the compact set of particles, they are both removed. This similarity was also discovered by Paterson (1984). It is important to emphasise that there is no one to one correspondence between both DLA

and anti-DLA processes and flow in porous media, but the resemblances are there and thus these models are important when trying to understand mechanisms that produces the flow patterns.

So far the capillary forces has been neglected, but in the case of capillary fingering this is the dominating force and the viscous forces are neglected. This is can be achieved by injecting a fluid at low rates into a defending fluid. The observed patterns have many resemblances with viscous fingering but some more clusters are formed, as illustrated in figure 2.11 a). Invasion percolation is a statistical theory aiming to describe this process (Wilkinson and Willemsen (1983)). The basic idea behind this is to let the invading fluid enter one tube at each time step. This tube will usually be the one with the biggest radius, and thus the invading fluid will choose the path of least resistance.

Chapter 3

Method

A lot of the contribution from this thesis lies in the numerical simulations that has been done, and the details of the implementations is therefore important. This section will present roughly how the theory from chapter 3 has been implemented to create realistic simulation of the flow phenomena.

3.1 Hexagonal Lattice of Tubes

A hexagonal network of tubes will be used as a simple model of the porous medium. Each intersection of three tubes is called a node and the number of nodes in the horizontal direction is denoted N while the number of nodes in the vertical direction is denoted M. In the case of figure 3.1 $N = 8$ and $M = 4$. The total number of nodes is given by

$$N_{\text{nodes}} = NM, \tag{3.1}$$

while the number of tubes is

$$N_{\text{tubes}} = \frac{3}{2}NM. \tag{3.2}$$

For simplicity the lengths of the tubes will all be the same in the networks used in the simulations, while randomness in the system will be incorporated by letting the radius vary. These will be uniformly random generated values between $r_{\min}$ and $r_{\max}$.

3.2 Boundary and Initial Conditions

The model will have periodic boundary conditions and a global pressure gradient in the vertical direction, responsible for pushing the fluids through the network. This means that the nodes to the left side will be connected to those on the right side, and the lower nodes connected to the upper nodes. A pressure gradient ΔP in the vertical direction will represents the driving force in the system. This pressure gradient will push the fluids upwards

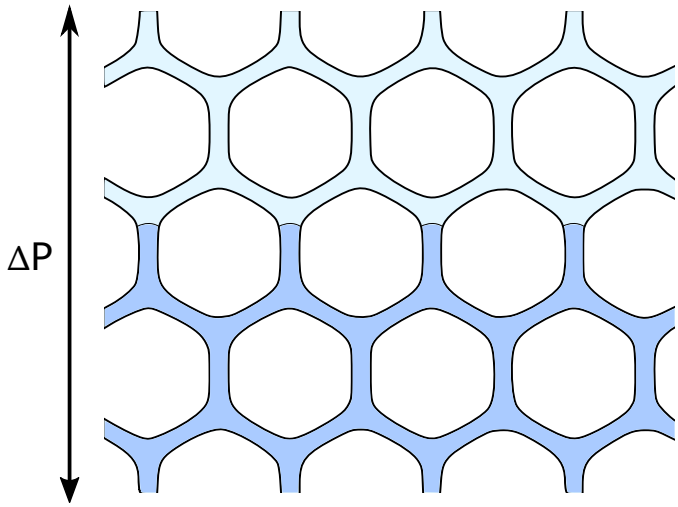

Figure 3.1: A typical hexagonal lattice that is used in the simulations. This illustrates an initial condition where the system is partially filled with non-wetting fluid. There is a pressure gradient in the vertical direction representing the driving force.

in the network. When the fluid reaches the top it will reenter at the bottom. These kind of boundary conditions was first used by Knudsen et al. (2002).

The system will be simulated for different saturation of non-wetting fluid. The saturation will be set by the initial condition. The tubes will be filled with non-wetting fluid from the bottom up, until the desired saturation is reached. This means that the beginning of each simulation the wetting and non-wetting fluid will be separated in two parts. The methodology that is described in this section is based on Aker et al. (1998). The pressure in an arbitrary node n_i can be found when imposing that the total flow through a node must be conserved. The flow through a tube connecting two nodes n_i and n_j can be expressed as

$$q_{ij} = g_{ij}(p_j - p_i - p_c + \delta_{ij}\Delta P), \tag{3.3}$$

Here q_{ij} is the flow and g_{ij} is the mobility of the tube connecting node i and j. The δ is zero unless the tube is crossing the vertical boundary, then it is 1. The term $\delta_{ij}\Delta P$ represent the pressure gradient driving the system. The conservation of flow can be expressed as

$$\sum_j q_{ij} = 0 \tag{3.4}$$

This is simply Kirchhoff's equation, where j runs over all the neighboring nodes of the i-th node. The index i runs over all nodes in the network. Substituting (3.4) into (3.3) and rearranging yields,

$$\sum_j g_{ij}(p_j - p_i - p_c + \delta_{ij}\Delta P) = 0. \tag{3.5}$$

By moving the p_c and $\delta_{ij}\Delta P$ terms to the right side the system can be written as a linear matrix equation on the form $\mathbf{A}\boldsymbol{p} = \boldsymbol{b}$ and solved with respect to $\boldsymbol{p}$ to find the pressure in every node. The elements of $\mathbf{A}$ will be the conductance while $\boldsymbol{b}$ will be a vector containing the capillary pressures as well as the external pressure due to the boundary conditions. The flow in each pipe can now be determined by (3.3). To solve the linear system of equations several algorithms can be used. In the general case $\mathbf{A}$ will vary for every time step. The conjugate gradient method will then be a good approach. In this work, the viscosities of the two phases are identical. This means that the matrix $\mathbf{A}$ will be constant, and thus it only needs to be inverted once. In this case the linear algebra library Armadillo (2016) was used to perform the inversion and the required matrix multiplications. A possible improvement could be to implement a Cholesky decomposition and use this to solve the equation. Both the Cholesky decomposition and the conjugate gradient method can be found in Press et al. (1996)

3.3 Updating the meniscus positions

In order to update the meniscus positions a time step Δt must be chosen. This is done by allowing the meniscus positions to move no longer than a given length $\Delta x_{\max}$. Denoting the flow velocity $v_{ij} = q_{ij}/A$, where A is the cross sectional area, the time step is calculated by,

$$\Delta t = \min_{ij} \left[\frac{\Delta x_{\max}}{v_{ij}} \right]. \tag{3.6}$$

This means that the time step is dependent on the local velocities in the tubes.

Once the time step and the flow in each tube is established it is easy to propagate the meniscus positions inside the tube. This can be done with a simple Euler algorithm,

$$x_{t+1} = x_t + v_{ij}\Delta t. \tag{3.7}$$

The value $\Delta x_{\max} = 0.1L$ will be used is the simulations. It has been verified that this is a sufficiently small time step (Knutson et al. (2001), Ramstad et al. (2009)).

3.3.1 Meniscus behaviour at nodes

A challenge in network simulators is to handle what happens when a meniscus reaches a node. It will take time for the meniscus to fill the pore volume, and during this filling process the other fluid can pass through the node. The following section will explain how this is handled in the simulations. The code uses a set of rules to mimic the actual behaviour of fluids, and has been developed by Morten Vassvik. What is presented here is a brief review of his work which not yet has been published.

In order to explain these rules, consider three tubes that are connected to the same node where different types of fluids are entering and exiting. This is the case for all figures a-h in 3.2. The first thing that happens is that the meniscus positions are propagated into the

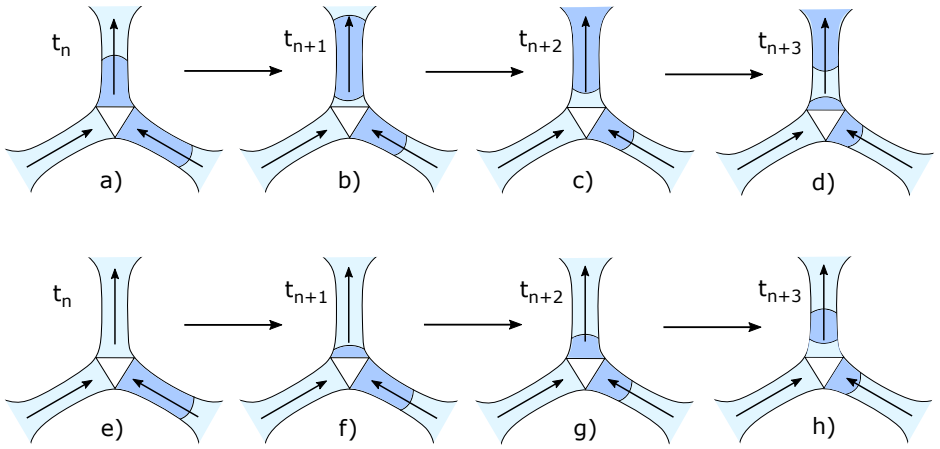

Figure 3.2: How the algorithm handles the case when different fluids flow into the same node. a-d illustrates what happens if the tube where the flow is leaving is filled with non-wetting fluid, while e-n shows the case where the same tube is filled with a wetting fluid.

node, and a fraction F_n which tells the amount of wetting and non-wetting fluid inside the node is calculated,

$$F_n = \frac{V_{\text{nw}}}{V}. \tag{3.8}$$

Here V_{nw} and V is respectively the volume of non-wetting fluid and total fluid volume. If only non-wetting fluid flow in to the node its value is 1, and if there is only wetting fluid flowing into the node, F_n is equal to 0. The next task is to distribute this fluid into the tubes where the flow is leaving the node. The way the simulation handles this will depend on the conditions in the tubes of outgoing flow. In particular, whether this tube throat is occupied by a small bubble or not. By small bubble means a bubble whose length is shorter or equal to the tube radius. Start by considering the case where there are no small bubbles in the tube of outgoing flow. This is shown in both 3.2a and b. If the tube is occupied by a wetting fluid, the wetting part of the F_n will be placed next to the wetting fluid that already exist in the tube and a non-wetting bubble will be created at the end of the tube (figure 3.2 b). If the tube of outgoing flow is occupied by a non-wetting fluid, the exactly opposite will happen and a wetting bubble will be created (figure 3.2 f).

Now a small bubble has been created in the tube of the outgoing flow. In the next iteration the non-wetting part of F_n will be added to the non-wetting bubble, but the bubble will still remain at the end of the tube. The wetting part in the node, will pass the non-wetting bubble and be added to the wetting part. (figure 3.2 c). The same holds in the case where the wetting and non-wetting fluids are switched (figure 3.2 g). This means that no new bubbles are created, and that the small bubbles are retained at the nodes until they have the same length as the tube radius. The only exception to this rule is if there is only one small bubble in the tube where the flow is leaving and the F_n is equal to zero or one. Then this bubble will be pushed through the tube.

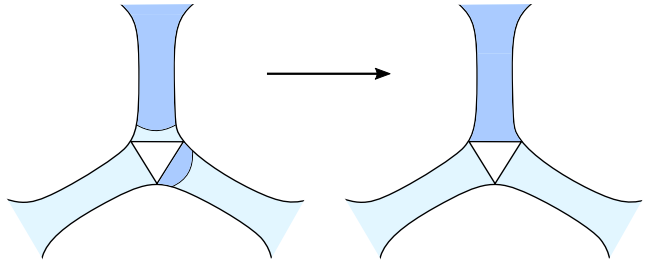

Figure 3.3: How the algorithm acts when two small bubbles of different wetting is located next to the same node

There is one additional rule in the algorithm. This rule was also originated from studying the filling process of a pore. When small bubbles of different types are located at the end of the tubes connected to the same node, these bubbles will switch place. This way, fluids of same types will stick together. Figure 3.3 illustrates this. In every step of this algorithm the volume of both phases will be conserved.

3.4 Case Studies

To investigate the effect of changing the tube geometry several cases will be studied. The first case will serve as a base case and its purpose will be to verify that the simulation is working as expected, and use it for comparison with other cases. The capillary pressure will be approximated by (2.13), and the tubes will be cylindrical. This is the same geometry as used by Aker (1996). The radii will be uniformly distributed between $0.1L$ and $0.4L$. The results will be studied by looking at the macroscopic properties of the flow. The actual distribution of the fluid throughout the network will also be visualized at different points in time.

Once it has been verified that that the simulation procedure is working as expected a second and third case will be done. Here different cross sections will be studied. In the second case an equilateral triangle will be used, and in the third case a narrow triangle where the two larger corner angles are twice as big as the small one. The geometry factors will be respectively 0.048 and 0.039. The radius if the inscribed circle in the tubes will be selected such that the single phase flow will be the same as for case 1. This is done so that it will be easy to compare the results for the different cases. The purpose of comparing these different cases is to verify that changing the cross section does not have a major impact on the results.

The second part will investigate how the radius shape of the tube affect the final result. This will be done by studying two cases, case 4 and case 5, where different radius func-

Case	Cross section	Capillary pressure
1	Circular	(2.13)
2	Equilateral triangle	(2.9)
3	Narrow triangle	(2.9)
4	Circular	(2.12) using radius function (2.14)
5	Circular	(2.12) using radius function (2.15)
6	Circular	(2.19)

Table 3.1: Summary of the different cases that will be studied in order to investigate the effects of tube geometry

tions are used. (2.12) will then determine the capillary pressure. These cases will be compared to each other as well as the base case. The purpose of doing this is to verify that (2.13) is a good approximation at small wetting angles, and investigate what happens as the wetting angle approaches 90°. Finally a sixth case will be studied. This is the case where the meniscus curvature is bounded due to the pore geometry. In previous work this effect has been neglected, and the purpose of doing this is to verify if that is a good approximation or not. Table 3.1 sums up all the different cases. In all these cases the values $\mu_1 = \mu_2 = 0.1\text{Pas}$ and $\gamma = 30\text{mN/m}$ will be used. The pressure gradient over the system will be constant and is chosen so that the pressure drop over each tube will be the same regardless of grid size. It is given by $\Delta P/M = 16.8\text{kN/m}^2$, where M is the number of nodes in the vertical direction.

3.5 Scaling of the network

The number of nodes used in the simulation may have impact on the final result, and to investigate how many nodes needed to avoid unwanted scaling effects a preliminary simulations with 10x10 (150 tubes), 30x30 (1350 tubes) and 60x60 nodes (5400 tubes) were done for comparison. The results for zero wetting angle is shown in 3.4. In order to make comparison simple all the flow-rates are normalized so that they all are equal to 1 at at minimum and maximum saturation. In the 10x10 case it is seen that the flow curve behaves quite different from what was seen for 30x30 nodes. It does drop to zero around $S = 0.4$ and is not very smooth. The reason why the flow drops to zero is that the capillary pressure is able to completely cancel out the external pressure gradient. The reason why this only happens at 10x10 nodes is that there are a fewer tubes, and the likelihood that the non-wetting fluid is able to ”block” every tube in a cross section is a lot bigger than when the node count is higher. When comparing the curves from 30x30 and 60x60 nodes, it is seen that they behave almost identical. By taking a closer look the 60x60 curve we see that it is slightly smoother that the one generated by 30x30 nodes. This is also reasonable because 5400 tubes is a much larger sample than 1350, and thus each radius will have smaller impact on the final results. both the large and medium lattices are free of the effects seen in the small grid and thus it is concluded that 30x30 nodes is sufficient.

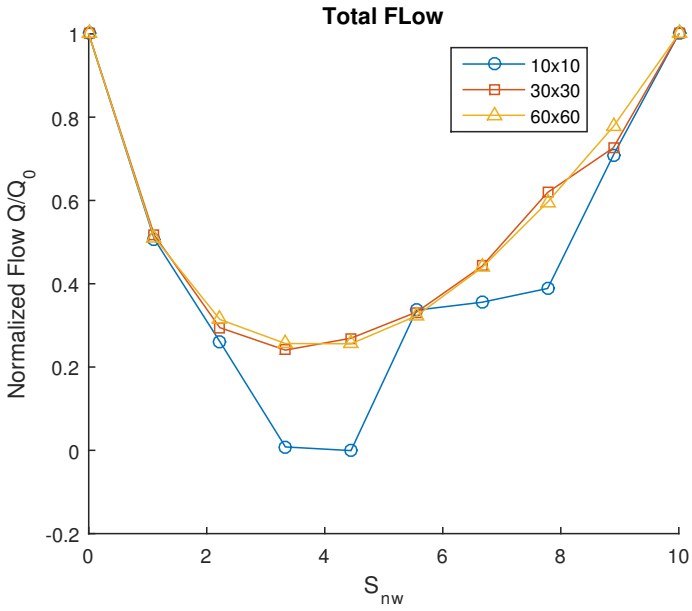

Figure 3.4: Comparison of flow rates for 10x10, 30x30 and 60x60 nodes.

Chapter 4

Results

This chapter will present the results of the simulations and a discussion. Several simulations have been performed to investigate what effect the cross section and tube radius have on the final result. This will be done by looking at the total and fractional flow as well as the capillary number, which has been defined in section 2.4.

The first part of this chapter will focus on verifying that the code is working as expected and point out important features of the resulting flow. This will correspond to case 1. The second part will study the impact of the tube geometry and compare the results with each other and case 1.

4.1 Time evolution of fluid front

Figure 4.1 visualizes the time evolution of case 1 where the non-wetting saturation is 0.4. There are 40 x 80 nodes, and the number of tubes is 4800. It is seen that the front of the non-wetting fluid is propagating in to the wetting, and thus this is similar to a drainage process. Due to the periodic boundary wetting fluid flows in to the bottom of the system and it replaces the non-wetting fluid. This is an imbibition process. We start looking at the propagating front. It is seen that the front is slowly moving upwards, while it is getting rougher. Some fingers of non-wetting fluid are observed moving ahead of the front while some of the wetting fluid gets trapped within the front.

In the withdrawing part of the non-wetting fluid, some of the same dynamics is seen, but there are certainly less fingers. Some amount of non-wetting fluid is left behind, forming small clusters. As the front reaches the boundary it reenters the system at the bottom, mixing the fluids. When this mixing has been going on for a while a steady state is reached, where the fluid distributions only fluctuates on a microscopic level while remains constant on the macroscopic scale. This is illustrated at $t = 45$.

Figure 4.2 shows the total flow, what fraction of the total flow that is due to the non-wetting fluid and the capillary number as function of time for the same system as shown

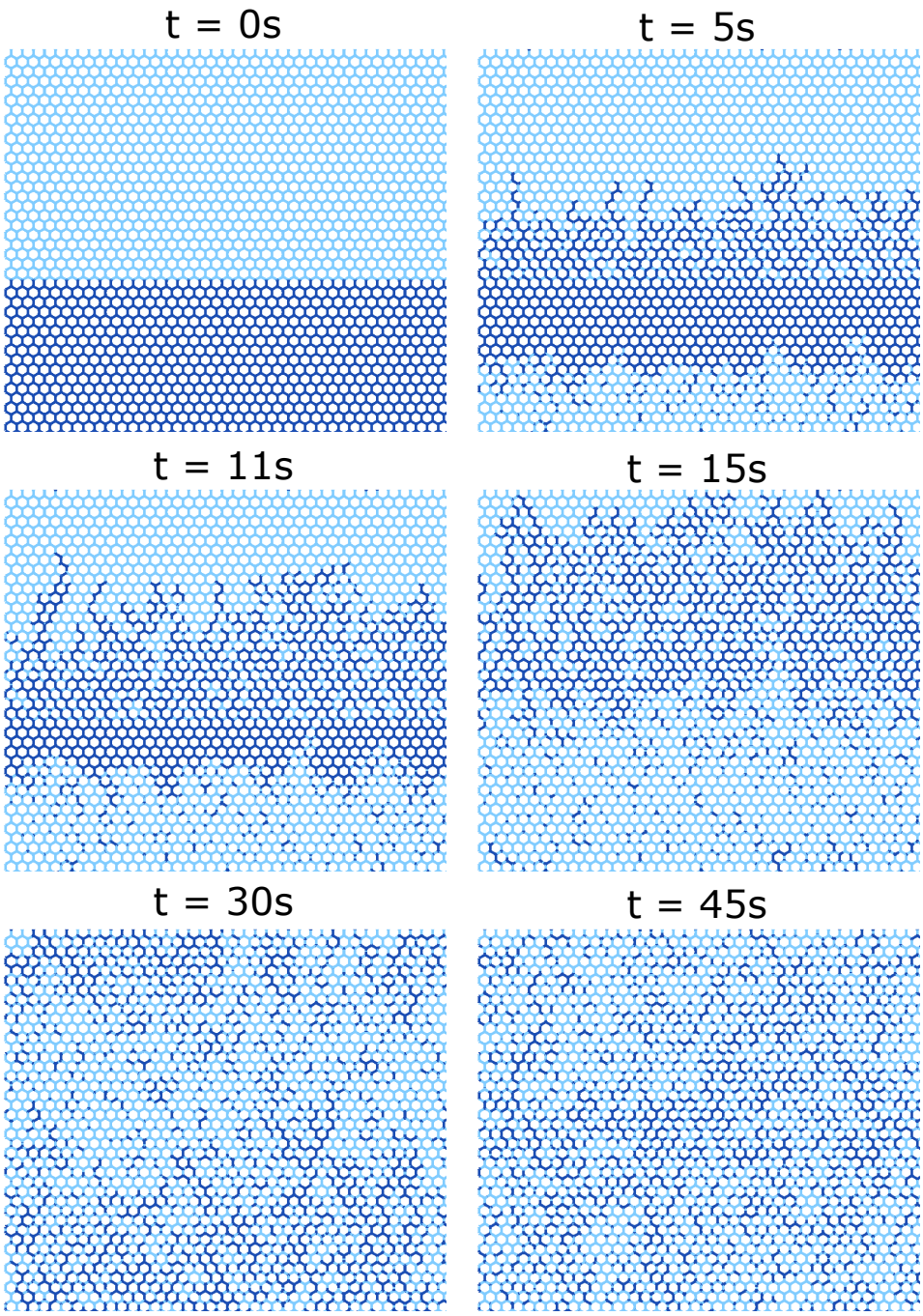

Figure 4.1: Time evolution of two phase flow. N is the number of iterations, and the top right system is the initial condition. The network consist of 40 X 80 nodes and has a saturation of 0.4.

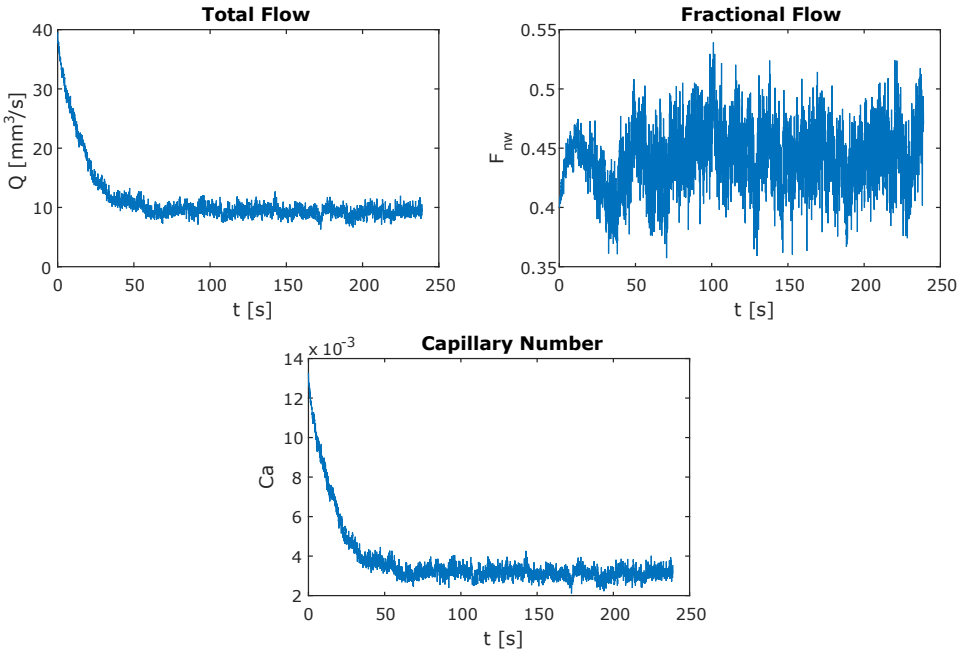

Figure 4.2: Time evolution of the total and fractional flow for a 40x80 grid.

in figure 4.1. It is seen that they both changes very rapidly in the beginning, while leveling out around an equilibrium with some fluctuations. This is in accordance with what was observed in figure 4.1.

The capillary number starts out at 1.3×10^{-2} and drops to 2.5×10^{-3} after a while. In terms of Lenormands phase diagram this means that the flow pattern should be somewhere in between capillary fingering and stable displacement. This agrees with the results, showing some fingers ahead of the fluid front. This also means that neither percolation theory or anti-DLA can be used to describe the invasion process seen in the beginning of the simulation. As seen in this section the system reaches a steady state value when the mixing process has been going on for long enough. For the rest of this chapter steady state values will be presented and discussed.

4.2 Macroscopic results

In the following section, the effects of tube cross section and radius will be studied. Results from cases 1-6 in table 3.1 will be presented as curves generated by changing the saturation and wetting angle. Ten different saturations and wetting angles have been used. All the simulations have been done on a 30x30 grid of nodes. The radius distribution is the same in all cases. Each simulation has been done for 50 000 iterations, and all the data points is found by taking the average value of the steady state.

The results from the base case is presented in figure 4.3. Looking at the total flow Q, it is seen that it has a strong dependence on S when the wetting angle is small, but it gradually moves toward a constant value as θ goes to 90°. The values for $S = 0$ and $S = 1$ is the same, regardless of θ This makes sense because in these cases there are only one fluid occupying the media, and thus there are no capillary forces. Looking at the expression for the capillary pressure (2.13), it is seen that it only depends on $\cos\theta$, and thus it vanishes as the wetting angle approaches 90°. This means that there are no capillary forces and the flow gets independent of the saturation. This is clearly unphysical because in a real porous media the tube walls are not straight, and thus the meniscus will have curvature even at 90° wetting angle. It is observed that the minimum point for all the curves are moved to the left.

The curves of wetting and non-wetting flow rates roughly increases and decreases at the saturation changes. It can be seen however that for small wetting angles, as the value decreases, it flattens out at a value unequal to zero, before it drops to zero at the endpoints. For wetting angles close to 90° the curves are almost linear. This is reasonable since there are no capillary forces, and the viscosity of the fluid are equal, meaning there is nothing that distinguish the fluids from each other. Several papers (e.g Wyckoff and Botset (1936), Øren et al. (1998)) have been investigating the relative permeabilities of porous media, and the permeability curves have many resemblances with the flow curves presented here. This is as expected because by looking at Darcys's law, the flow is directly proportional to the permeability when the pressure gradient and viscosity remains constant.

The fractional flow is for small wetting angles S-shaped, and crosses the straight line between 0 and 1 at approximately 0.4. This is what it observed in simulations done by others as well (e.g Knudsen et al. (2002)). And again, as the wetting angle approaches 90 °, the fluids have equal properties and, the fraction between them is almost directly proportional to the saturation.

4.3 Varying the cross section

Two set of simulations have been done with tubes of triangular cross section corresponding to case 2 and 3. In case 2 an equilateral triangle were used, while in the case 3 a narrow triangle where two corner was set to 75° and the last one to 30°. The geometry factors were respectively 0.048 and 0.039. In figure 4.4 the total and fractional flow for both cases is plotted next to case 1 for a wetting angle of 54°. It is seen that the shape of the curves are almost identical, but they are scaled differently. This is as expected since in the expressions for the capillary pressure for circular (2.11) and triangular (2.12) tubes, the only difference is a geometry-dependent scaling factor. When looking at the flow fraction this is confirmed, as they are almost identical for all the three cases.

One may be surprised that the cross-sectional shape of the tube does not have more impact on the result. The reason for this may be the fact that thin film flow has been neglected. For tubes with sharp corners thin film flow will be significant, and thus in a more realistic system, the differences would probably be larger.

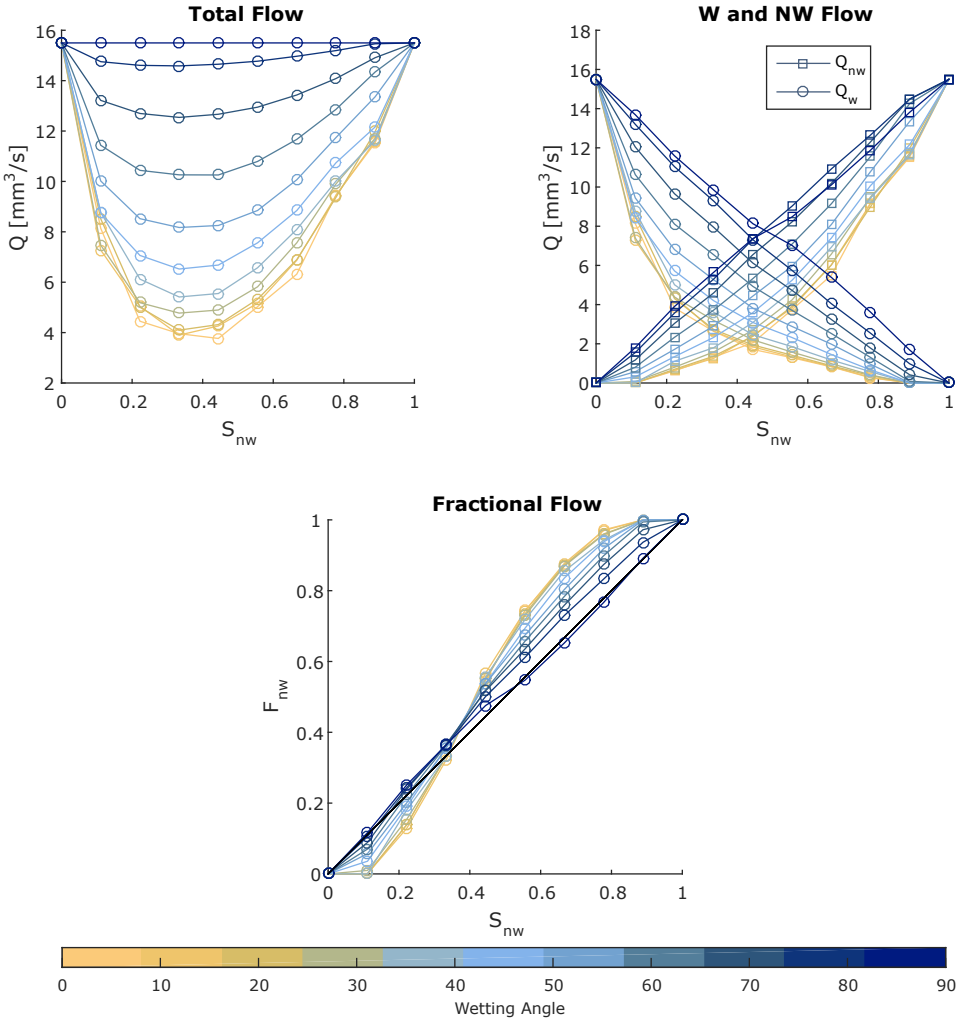

Figure 4.3: Results from case 1, varying saturation and wetting angles. The total and fractional flow is plotted.

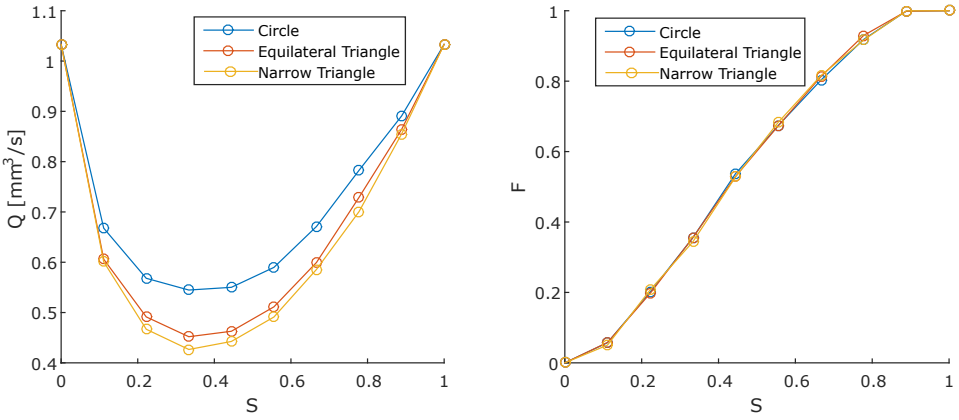

Figure 4.4: Total and fractional flow plotted at 54° wetting angle, for case 1, 2 and 3.

4.4 Varying the radius

So far the capillary pressure with respect to the position of the meniscus has been assumed to follow the approximation (2.13). As illustrated in the theory section this is not a realistic approximation when the wetting angle gets large. These effects will be studied in this section, and simulations where the capillary pressure obeys (2.12) and (2.19). This corresponds to case 4 and 5.

Figure 4.5 shows the results from case 4. The most remarkable difference is that for wetting angles close to 90° the flow does not become constant, but is still dependent on the saturation. This is as expected since the p_c now never drops to zero throughout the tube. The lines are packed more closely together, showing that the dependence of θ is not as significant as for case 1. It is interesting to see that for $\theta = 90°$ the total flow curve becomes symmetric about the line $S_{nw} = 0.5$. This is reasonable because the wetting angles of the fluids are the same, and thus they should behave identical. Apart from this, the features of this result is approximately the same as in case 1.

The result of simulations from case 5 had many resemblances with case 4. Flow curves for case 5 have been plotted in figure 4.6 a). The flow at zero wetting angle is slightly larger than in case 4, and the minimum point is pushed further to the right. At 90° wetting angle the flow is almost identical in both case 4 and 5. This indicates that the actual shape of the radius function is not so important.

Case 6, where the radius of the meniscus was bound by an upper limit had quite similar results as case 5. However there were some differences, as seen in figure 4.6. We see that the flow is larger than in case 5 at zero wetting angle. This may be because the capillary pressure is not allowed to drop to zero in the nodes, and thus the difference between the maximum and minimum capillary pressure a bubble experiences when traveling through the media is smaller. Figure 4.7 compares the fractional flow for case 5 and 6 at

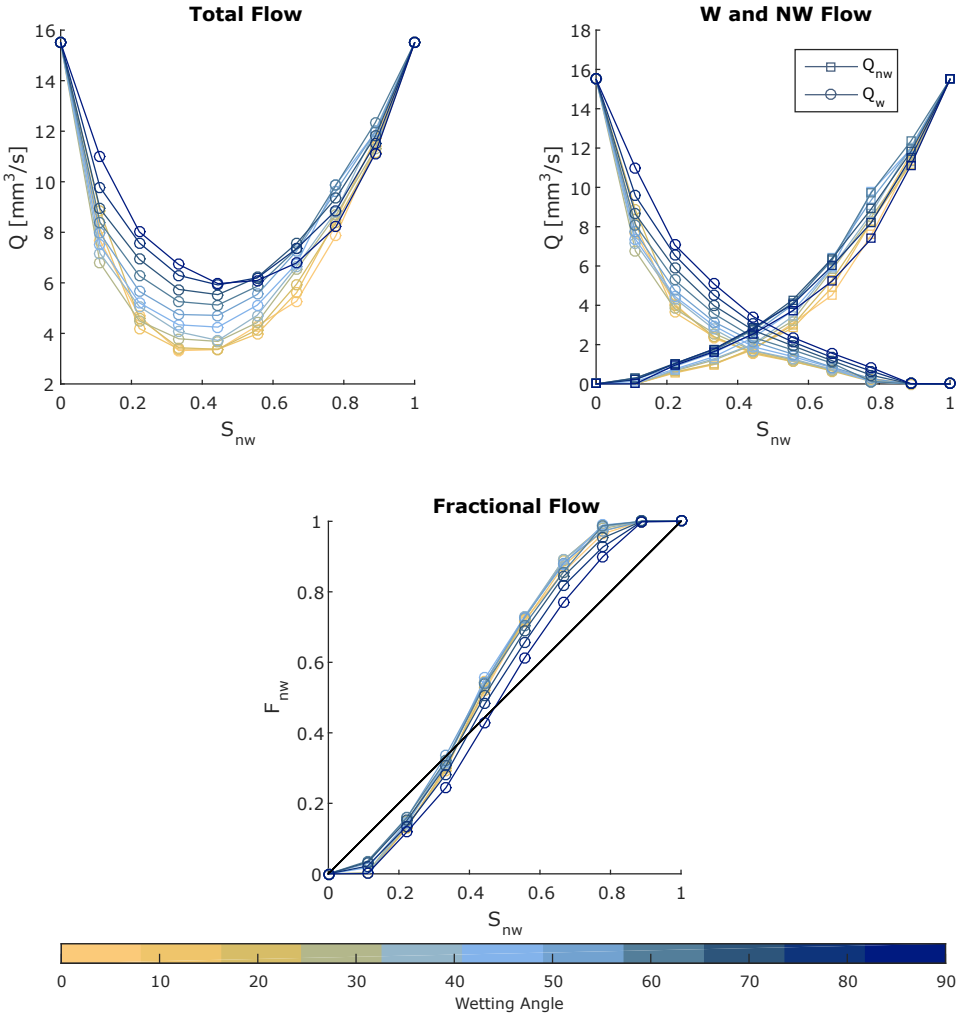

Figure 4.5: Results from case 4. The total and fractional flow is plotted, as well as the wetting and non-wetting flow.

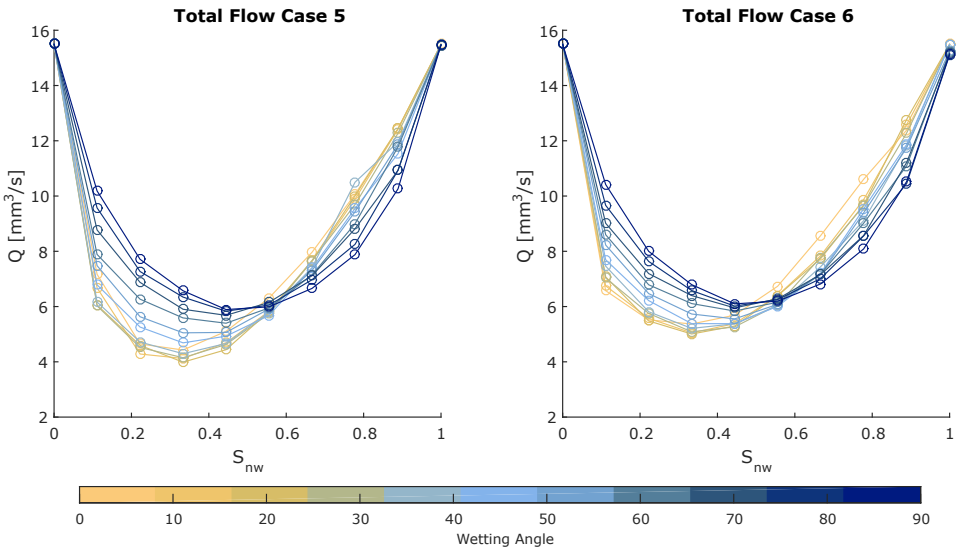

Figure 4.6: Total flow for case 5 and 6

$\theta = 36°$. It is seen that the curve from case 5 remains constant at zero and one longer than in case 6. This happens when either the saturation is small or large. This may indicate that bubbles easier get stuck in the nodes when the capillary pressure drop to zero than in the case where the capillary pressure has a lower bound.

Figure 4.8 compares the total and fractional flow curves for case 1, 4, 5 and 6 at zero wetting angle. It is seen that the flow curves all are quite similar, but their shapes varies slightly. This indicates that the approximation in case 1 is good at small wetting angles. This is also true when looking at the fractional flow which is very similar in all three cases. The major difference happens as the wetting angle grows towards 90 °. Then the approximation done in case 1 becomes less accurate and differs a lot from case 4, 5 and 6 where the slope of the tube is taken into account when calculating the capillary pressure.

When comparing case 4, 5 and 6 some differences are seen but it is hard to verify which one is most physically correct. In order to determine this, experiments with similar conditions should be done. This is however challenging and time demanding. Changing the wetting angle in the simulation takes a second while doing the same for an experiment would probably mean creating a new system with different material. A more viable approach would be to do a both lattice Boltzmann and network simulations on a small set of nodes, and compare these to each other. This would help validating the different assumptions made in the network model.

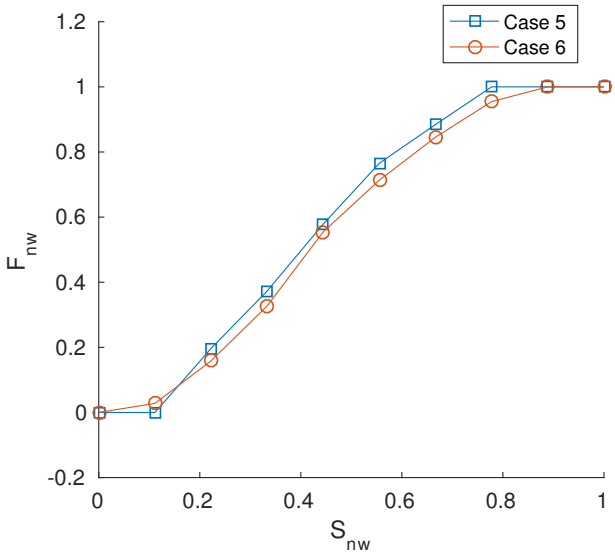

Figure 4.7: Fractional flow for case 5 and 6 at $\theta = 36°$.

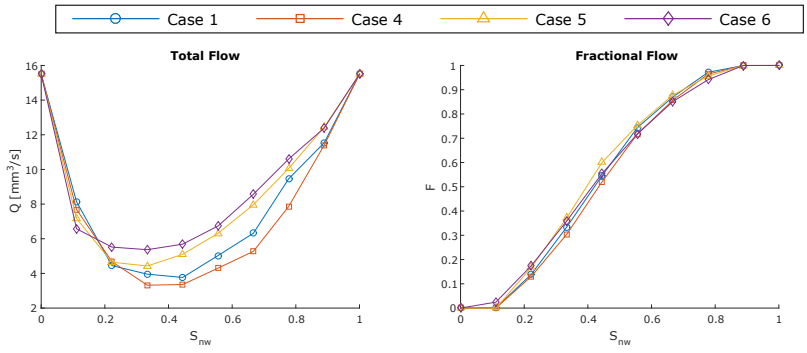

Figure 4.8: Comparison of total flow and fractional flow at $\theta = 0$ for case 1, 4, 5 and 6

Chapter 5

Conclusion

In this work a simple network model has been used to study two phase flow in porous media. The purpose of this work was to study what impact the tube geometry have on the capillary pressure in the tubes that models the media. A simulation procedure based on Aker et al. (1998) was implemented for a two dimensional hexagonal lattice. In total six different cases was studied. The first case was a simulation with parameters used in previous papers. The purpose of this case was to verify that the simulation procedure was working as it should, and be used for comparison with other cases. This case was compared with two other cases where triangular cross sections of different shape was used. It was seen that the flow dependence on the saturation S_{nw} and wetting angle θ was almost the same in all cases, but they were scaled slightly differently. This was as expected since changing the cross-section corresponds to changing the permeability of each tube. Because of this it can be concluded that the cross section has little impact on the final result. It is important to mention that in this model thin film flow was neglected.

The behaviour of the meniscus inside a tube with a varying radius was then studied. In previous papers an approximate capillary pressure was used. To investigate if this approximation is a good one, a fourth case was done where a more realistic expression was derived by taking the slope of the tube into account. The radius expression that were used was diverging towards the end of the tube. Simulation results showed that for small wetting angles the approximation in case 1 and the capillary pressure in case 4 acted the same. When the wetting angle was moving towards 90° the results was differing a lot. Based on this it is concluded that the approximation is good for small wetting angles, but bad when the wetting angle increases. To see if the actual radius shape had significant impact a fifth case was done. This time the radius was modeled as the distance between two semicircles. It was observed some differences between case 4 and 5, but lacking experiments and other means of verification made it hard to conclude which one is the most physically correct.

Geometrical considerations showed that the capillary pressure difference in many cases is bounded by the narrow space inside the pores. A new expression trying to take this into account was derived, and a sixth case was done to investigate if this had any effect. The results had many resemblances with the ones from earlier cases, but some differences

were observed. The most notable one was that bubbles easier got stuck at low and high saturations in case 5 than 6.

A big challenge when validating the results of this work is to find experiments to compare with. Lots of studies have been done on drainage and imbibition processes, but there has been done little experimental work on the mixing processes studied in this thesis. It would also be very valuable to have Lattice Boltzmann simulations to compare with. This could help verify the behaviour of the network model. Thin film flow has been neglected throughout this work. It would be valuable to have more research on how this impacts the results, especially when the tubes in the network have sharp corners.

Bibliography

Aker, E., 1996. A simulation model for two-phase flow in porous media. University of Oslo, Department of Physics.

Aker, E., Måløy, K. J., Hansen, A., Batrouni, G. G., 1998. A two-dimensional network simulator for two-phase flow in porous media. Transport in Porous Media 32 (2), 163–186.

Armadillo, 2016. C++ linear algebra library. [Accessed December 12, 2016].
URL `http://arma.sourceforge.net/`

Dias, M. M., Payatakes, A. C., 1986. Network models for two-phase flow in porous media part 1. immiscible microdisplacement of non-wetting fluids. Journal of Fluid Mechanics 164, 305–336.

Fatt, I., et al., 1956. The network model of porous media.

Fenwick, D. H., Blunt, M. J., et al., 1998. Network modeling of three-phase flow in porous media. SPE Journal 3 (01), 86–96.

Joekar-Niasar, V., Hassanizadeh, S., 2012. Analysis of fundamentals of two-phase flow in porous media using dynamic pore-network models: A review. Critical reviews in environmental science and technology 42 (18), 1895–1976.

Knudsen, H. A., Aker, E., Hansen, A., 2002. Bulk flow regimes and fractional flow in 2d porous media by numerical simulations. Transport in Porous Media 47 (1), 99–121.

Knudsen, H. A., Hansen, A., 2002. Relation between pressure and fractional flow in two-phase flow in porous media. Physical Review E 65 (5), 056310.

Knutson, C. E., Werth, C. J., Valocchi, A. J., 2001. Pore-scale modeling of dissolution from variably distributed nonaqueous phase liquid blobs. Water Resources Research 37 (12), 2951–2963.

Lenormand, R., Touboul, E., Zarcone, C., 1988. Numerical models and experiments on immiscible displacements in porous media. Journal of fluid mechanics 189, 165–187.

Lenormand, R., Zarcone, C., Sarr, A., 1983. Mechanisms of the displacement of one fluid by another in a network of capillary ducts. Journal of Fluid Mechanics 135, 337–353.

Man, H., Jing, X., 2000. Pore network modelling of electrical resistivity and capillary pressure characteristics. Transport in Porous Media 41 (3), 263–285.

Martys, N. S., Hagedorn, J. G., 2002. Multiscale modeling of fluid transport in heterogeneous materials using discrete boltzmann methods. Materials and structures 35 (10), 650–658.

Mason, G., Morrow, N. R., 1991. Capillary behavior of a perfectly wetting liquid in irregular triangular tubes. Journal of Colloid and Interface Science 141 (1), 262–274.

Oh, S. G., Slattery, J. C., et al., 1979. Interfacial tension required for significant displacement of residual oil. Society of Petroleum Engineers Journal 19 (02), 83–96.

Øren, P.-E., Bakke, S., 2002. Process based reconstruction of sandstones and prediction of transport properties. Transport in Porous Media 46 (2-3), 311–343.

Øren, P.-E., Bakke, S., Arntzen, O. J., et al., 1998. Extending predictive capabilities to network models. SPE journal 3 (04), 324–336.

Paterson, L., 1984. Diffusion-limited aggregation and two-fluid displacements in porous media. Physical review letters 52 (18), 1621.

Patzek, T., Silin, D., 2001. Shape factor and hydraulic conductance in noncircular capillaries: I. one-phase creeping flow. Journal of colloid and interface science 236 (2), 295–304.

Press, W. H., Teukolsky, S. A., Vetterling, W. T., Flannery, B. P., 1996. Numerical recipes in C. Vol. 2. Cambridge university press Cambridge.

Ramstad, T., Hansen, A., Øren, P.-E., 2009. Flux-dependent percolation transition in immiscible two-phase flows in porous media. Physical Review E 79 (3), 036310.

Sahimi, M., 2011. Flow and transport in porous media and fractured rock: from classical methods to modern approaches. John Wiley & Sons.

Schlumberger, 2007. Fundamentals of wettability. Accessed November 28, 2016.
URL https://www.slb.com/~/media/Files/resources/oilfield_review/ors07/sum07/p44_61.pdf

Sinha, P. K., Wang, C.-Y., 2007. Pore-network modeling of liquid water transport in gas diffusion layer of a polymer electrolyte fuel cell. Electrochimica Acta 52 (28), 7936–7945.

The New York Times, 2016. Rural water, not city smog, may be chinas pollution nightmare. Accessed December 13, 2016.
URL http://www.nytimes.com/2016/04/12/world/asia/china-underground-water-pollution.html

Valavanides, M., Constantinides, G., Payatakes, A., 1998. Mechanistic model of steady-state two-phase flow in porous media based on ganglion dynamics. Transport in Porous Media 30 (3), 267–299.

Washburn, E. W., 1921. The dynamics of capillary flow. Physical review 17 (3), 273.

White, F., 2011. Fluid Mechanics.

Wilkinson, D., Willemsen, J. F., 1983. Invasion percolation: a new form of percolation theory. Journal of Physics A: Mathematical and General 16 (14), 3365.

Wyckoff, R., Botset, H., 1936. The flow of gas-liquid mixtures through unconsolidated sands. Journal of Applied Physics 7 (9), 325–345.

Appendix A

A1

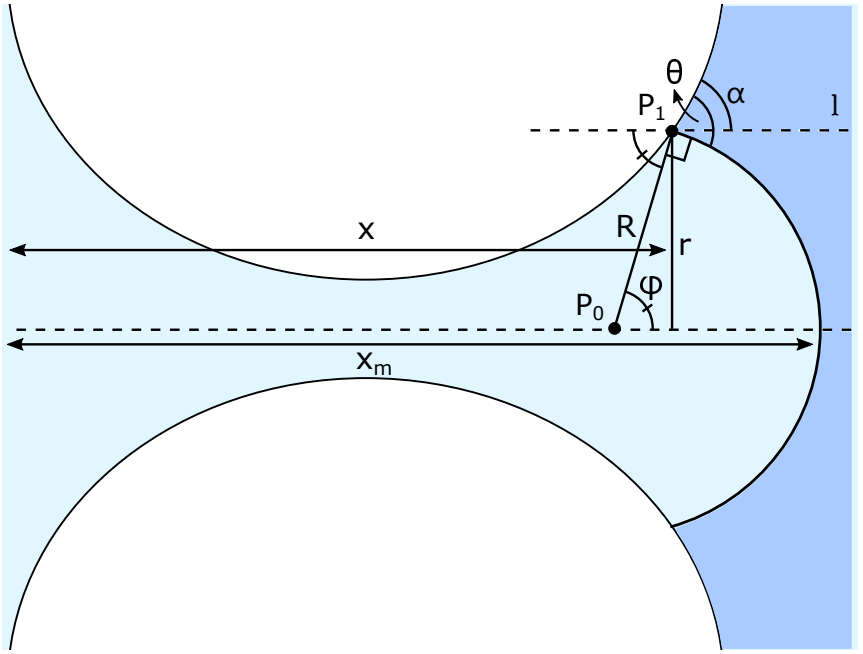

Figure 1: Parameters used to find the position of the center of the meniscus in a tube.

Consider the parameters in figure 1. The goal is to find the distance from the start of the tube to the center of the meniscus, x_m. This is to be expressed by the x-coordinate which is where the meniscus intersects with the tube and the wetting angle. The tube radius is given by an arbitrary function $r(x)$. Assume no gravity and that the meniscus circular. The center of the meniscus is denoted P_1 while the intersection point between the meniscus and the tube is denoted P_2. The line l is parallel with the x-axis and intersects the tube at the point P_1. In order to find this distance we must first find the angle ϕ between the x-axis and the line segment P_1P_2. This is equal to the angle between P_1P_2 and l. This can be found by summing up all the angles along the horizontal line intersecting with the

tube at point P and equate them to pi.

$$\theta - \alpha + \frac{\pi}{2} + \phi = \pi. \tag{1}$$

Rearranging yields

$$\phi = \alpha - \theta + \frac{\pi}{2} \tag{2}$$

The distance between x and x_m can now be found.

$$x_m - x = R(1 - \cos\phi). \tag{3}$$

Rearranging and substituting equation (2.10) for R and (2) for ϕ, yields

$$x_m = x + \frac{1 - \sin(\theta - \alpha(x))}{\cos(\theta - \alpha(x))} r(x) \tag{4}$$

A2

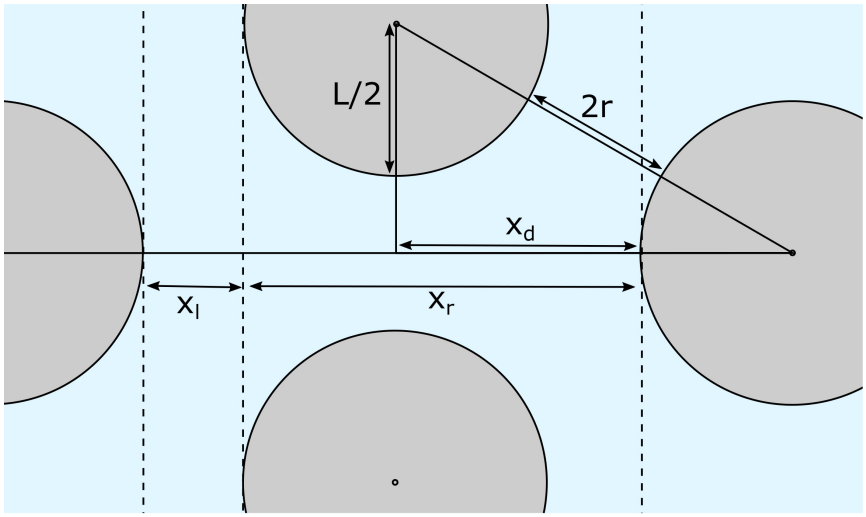

Figure 2: Parameters used to find the width of a pore space between three circular objects.

The maximum value x_m is allowed to have is given by the distance x_d. This distance can be found by using Pythagoras theorem, as illustrated in figure 2. The distance from the center of the tube to the maximum point is given by.

$$(L + 2\bar{r})^2 = (L/2 + \bar{r})^2 + (L/2 + x_d)^2. \tag{5}$$

The solution with respect to x_d is then given by

$$x_d = \sqrt{3}(L/2 + \bar{r}) - L/2. \tag{6}$$

Since the origin of the coordinate system in the tube is at the left endpoint, the distance to the left is

$$x_l = x_d - L/2 \tag{7}$$

and to the right

$$x_r = x_d + L/2. \tag{8}$$